



The spatial distribution of impact craters on Ryugu

Hirata, Naoyuki ; Morota, Tomokatsu ; Cho, Yuichiro ; Kanamaru, Masanori ; Watanabe, Sei-ichiro ; Sugita, Seiji ; Hirata, Naru ;...

(Citation)

Icarus, 338:113527

(Issue Date)

2019-11-05

(Resource Type)

journal article

(Version)

Accepted Manuscript

(Rights)

© 2019 Elsevier B.V.

This manuscript version is made available under the CC-BY-NC-ND 4.0 license

<http://creativecommons.org/licenses/by-nc-nd/4.0/>

(URL)

<https://hdl.handle.net/20.500.14094/90006493>



1 Title

2 **The spatial distribution of impact craters on Ryugu**

3

4 Authors

5 Naoyuki Hirata ^{a, *}, Tomokatsu Morota ^b, Yuichiro Cho ^b, Masanori
6 Kanamaru ^c, Sei-ichiro Watanabe ^d, Seiji Sugita ^{b, e}, Naru Hirata ^f, Yukio
7 Yamamoto ^g, Rina Noguchi ^g, Yuri Shimaki ^g, Eri Tatsumi ^{b, h}, Kazuo Yoshioka
8 ⁱ, Hirotaka Sawada ^g, Yasuhiro Yokota ^{g, j}, Naoya Sakatani ^g, Masahiko
9 Hayakawa ^g, Moe Matsuoka ^g, Rie Honda ^j, Shingo Kameda ^k, Manabu
10 Yamada ^e, Toru Kouyama ^l, Hidehiko Suzuki ^m, Chikatoshi Honda ^f,
11 Kazunori Ogawa ^a, Yuichi Tsuda ^g, Makoto Yoshikawa ^g, Takanao Saiki ^g,
12 Satoshi Tanaka ^g, Fuyuto Terui ^g, Satoru Nakazawa ^g, Shota Kikuchi ^g,
13 Tomohiro Yamaguchi ^{g, n}, Naoko Ogawa ^g, Go Ono ^o, Yuya Mimasu ^g, Kent
14 Yoshikawa ^o, Tadateru Takahashi ^g, Yuto Takei ^g, Atsushi Fujii ^g, Hiroshi
15 Takeuchi ^g, Tatsuaki Okada ^g, Kei Shirai ^g, Yu-ichi Iijima ^p.

16

17 * Corresponding Author E-mail address: hirata@tiger.kobe-u.ac.jp

18 **Authors' affiliation**

19 ^a Department of Planetology, Kobe University, Kobe 657-8501, Japan.

20 ^b Graduate School of Science, University of Tokyo, Tokyo 113-0033, Japan.

21 ^c Department of Earth and Space Science, Osaka University, Osaka 560-0043,
22 Japan.

23 ^d Graduate School of Environmental Studies, Nagoya University, Nagoya
24 464-8601, Japan.

25 ^e Planetary Exploration Res. Center, Chiba Institute of Technology,
26 Narashino 275-0016, Japan.

27 ^f University of Aizu, Aizu-Wakamatsu 965-8580, Japan.

28 ^g Institute of Space and Astronautical Science, JAXA, Sagamihara 252-5210,
29 Japan.

30 ^h Instituto de Astrofísica de Canarias, University of La Laguna, Tenerife,
31 E38205, Spain.

32 ⁱ Graduate School of Frontier Sciences, University of Tokyo, Kashiwa
33 277-8561, Japan.

34 ^j Kochi University, Kochi 780-8520, Japan.

35 ^k College of Science, Rikkyo University, Tokyo 171-8501, Japan.

36 ^l National Institute of Advanced Industrial Science and Technology, Tokyo
37 135-0064, Japan.

38 ^m Meiji University, Kanagawa 214-8571, Japan.

39 ⁿ Mitsubishi Electric Corporation, Kamakura 247-8520, Japan.

40 ^o Research and Development Directorate, JAXA, Sagamihara 252-5210,
41 Japan.

42 ^p Deceased

43

44 **Proposed Running Head:** Craters on Ryugu

45 Editorial Correspondence to:

46 Dr. Naoyuki Hirata

47 Kobe University, Rokkodai 1-1 657-8501

48 Tel/Fax +81-7-8803-6566

49

50 **Key Words**

51 Asteroid

52 Impact processes

53 Geological processes

54 **Highlights**

- 55 ■ We examined the spatial distribution of impact craters on Ryugu
- 56 ■ We completed a global impact crater catalogue of Ryugu (D>20 m)
- 57 ■ Crater density variations cannot be explained by the randomness of
58 cratering
- 59 ■ More craters are seen at lower latitudes and less at higher latitudes
- 60 ■ There are fewer craters in the western bulge and more around the
61 meridian

62

63 **Abstract**

64 Asteroid 162173 Ryugu has numerous craters. The initial
65 measurement of impact craters on Ryugu, by Sugita et al. (2019), is based on
66 Hayabusa2 ONC images obtained during the first month after the arrival of
67 Hayabusa2 in June 2018. Utilizing new images taken until February 2019,
68 we constructed a global impact crater catalogue of Ryugu, which includes all
69 craters larger than 20 m in diameter on the surface of Ryugu. As a result, we
70 identified 77 craters on the surface of Ryugu. Ryugu shows variation in
71 crater density which cannot be explained by the randomness of cratering;
72 there are more craters at lower latitudes and fewer at higher latitudes, and
73 fewer craters in the western bulge (160°E – 290°E) than in the region around
74 the meridian (300°E – 30°E). This variation implies a complicated geologic
75 history for Ryugu. It seems that the variation in crater density indicates that

76 the equatorial ridge located in the western hemisphere is relatively young,
77 while that located in the eastern hemisphere is a fossil structure formed
78 during the short rotational period in the distant past.

79 1. Introduction

80 Ryugu is a top-shaped asteroid with a mean radius of 448 m and a
81 rotational obliquity of 8 degrees (Watanabe et al., 2019). Since JAXA's
82 Hayabusa2 spacecraft arrived at asteroid 162173, Ryugu, on June 27, 2018,
83 the onboard optical navigation cameras (ONC) have obtained numerous
84 images of Ryugu and revealed many surface features, including abundant
85 impact craters (Sugita et al., 2019). This cratering suggests that a major
86 process in the formation of the surface of Ryugu has been via impacts from
87 other bodies. The low bulk density of Ryugu implies that the asteroid is
88 composed of fragments that probably resulted from catastrophic disruption
89 (Watanabe et al., 2019). The initial report of impact craters on Ryugu (Sugita
90 et al. 2019) was produced via the utilization of ONC images from July to
91 August 1, 2018, which identified approximately 30 impact craters from the
92 limited coverage of Ryugu. The surface crater retention age was estimated to
93 be in the order of 10^7 or 10^8 years, based on the number density of craters of
94 100 – 200 m in diameter (D). In addition, Sugita et al. (2019) reported that
95 the crater size-frequency distribution (CSFD) of Ryugu shows a lack of small
96 craters ($D < 100$ m), which indicates that the average resurfacing of the top
97 ~1-meter layer on Ryugu takes less than 10^6 years. Ryugu has a west/east
98 dichotomy (Sugita et al. 2019); its western side, the so-called western bulge,
99 ($160^\circ\text{E} - 290^\circ\text{E}$), has a high albedo, a low number density of large boulders,
100 is topographically high, and has a bluish color as compared to the eastern
101 side. The equatorial ridge located in the eastern hemisphere is slightly offset
102 towards the south.

103 The main purpose of this paper is (i) to present the basic information
104 (the location and size of each craters), which is not listed in the initial report
105 by Sugita et al. (2019), (ii) to accomplish a global catalogue of all the craters
106 ($D \geq 10 - 20$ m), utilizing additional images acquired after the publication by
107 Sugita et al. (2019) which have allowed the investigation of craters over the
108 entire surface of Ryugu, (iii) to investigate the statistical significance of the
109 spatial distribution of the impact craters. Note that we do not discuss the
110 crater size-frequency distribution or the depletion and retention time of
111 small craters, as these topics will be included in Morota et al. (in
112 preparation).

113

114 **2. DATA and Method**

115 **2.1. Crater counting**

116 This study utilized 340 ONC images for crater counting (Table 1): (i)
117 96 images obtained in July 20 2018 with a ground resolution of 0.72 m/pixel
118 providing global coverage excluding the polar regions > 70 degrees, (ii) 85
119 images obtained on August 1 2018 with a resolution of 0.69-0.55 m/pixel,
120 providing regional coverage of low latitudes < 40 degrees, (iii) 11 images
121 obtained on October 4 2018 with a resolution of 0.32 m/pixel, providing
122 coverage of the north pole, (iv) 18 images on October 30 2018 with a
123 resolution of 0.62 m/pixel providing coverage of the north and south poles (v)
124 26 images obtained on February 28 2019 with a resolution of 0.67 m/pixel
125 providing coverage of the north and south poles, (vi) 52 images obtained on
126 August 23 2018 with a resolution of 2.6 m/pixel providing coverage of the

127 south pole, (vii) 52 images obtained on January 24 2019 with a resolution of
128 2.1 m/pixel providing coverage of the north pole. Because the Hayabusa 2
129 spacecraft is generally remaining in the same position above the sub-Earth
130 point of the asteroid's surface and the rotational obliquity of Ryugu is small,
131 the emission angles of the images (i)-(v) are large for polar regions. The
132 low-emission images of Ryugu's polar regions, (vi) and (vii), were obtained at
133 a position distant from the equatorial plane. All of the impact craters were
134 identified from these ONC images. These ONC images will be freely
135 available at the end of 2020. Craters with diameters larger than 10-20 m
136 could be clearly identified as these images had a resolution of at least 10
137 pixels (though they had a resolution of less than 10 pixels in the case of the
138 image subset (iv)). We note that the choice of the minimum pixel number for
139 reliable crater identification requires care; it varies substantially depending
140 on imaging conditions, such as solar incidence angle. Also, stereo pair images
141 greatly improve the robustness of crater identification. Because the
142 Hayabusa2 ONC image dataset used in this study covers almost entire
143 surface of Ryugu with multiple imaging and large solar incidence angles, 10
144 pixel is sufficient for identifying craters on Ryugu. The images enabled us to
145 identify all impact craters exceeding 10 – 20 meters diameter over the entire
146 surface of Ryugu. Therefore, to ensure that crater counting was not affected
147 by image resolution, $D = 20$ m was set as the minimum diameter threshold.

148 We identified all circular or quasi-circular depressions as craters for
149 this study. This included cases where the circular depression lacked a raised
150 rim. However, we did not regard circular features without topographic

151 depressions as craters. Features such as topographic depression or rims were
152 judged from (i) the shape model of Ryugu (Watanabe et al. 2019), (ii) visual
153 observation using stereo pairs and (iii) visual observation based on shading
154 of images at low sun. Based on these criteria, we classified all the candidate
155 craters into types: I-IV (as summarized in Table 2). We judged those
156 classified as types I-III to be distinct crater (Nos. 1- 77 in Figure 1), and
157 classification IV to be less-distinct crater. For this study, we assumed that
158 type IV phenomena are not craters (Nos. 78-86 in Figure 1), and therefore
159 these were not included in crater density and statistical analysis.
160 Nonetheless, many craters were more or less degraded and infilled with
161 regolith or boulders and often lacked distinct shape, and this interpretation
162 was therefore often ambiguous.

163 To measure the size, latitude, and longitude of each crater we utilized
164 the Small Body Mapping Tool (Kahn et al., 2011), a global image mosaic map
165 of Ryugu, and a shape model of Ryugu. The global image mosaic map was
166 built from the ONC images, and the shape model was derived from
167 Watanabe et al. (2019). The Small Body Mapping Tool was used to measure
168 the diameters and locations of the craters for the study. This software
169 enabled measurement of the centers and diameters of craters based on three
170 points selected along the crater rim from a global mosaic map rendered onto
171 the shape model.

172 A fairly accurate surface area is required to obtain the number
173 density of the craters. In the case of an irregular-shaped asteroid, the
174 definition of the surface area is complicated. When defining it from a shape

175 model, the surface area increases infinitely as the resolution of the shape
176 model increases. To simplify, the surface area was not determined as the
177 total area of the surface polygons composing the shape model, but was
178 instead calculated as the surface of a sphere with a radius of 448 m. The total
179 surface area of Ryugu was thus calculated to be 2.5 km². We note that the
180 shape model of Ryugu (SHAPE_SFM_200k_v20180804.obj), which describes
181 Ryugu as 196608 plates, has the surface area of 2.77 km².

182 **2.2. The statistical analysis of the spatial distribution**

183 A statistical test was then performed to evaluate the significance of
184 variations in the crater density. The nearest-neighbor analysis was thus used
185 to discover whether the variation can be explained merely by randomness,
186 following the methodology of Squyres et al. (1997). The distance between
187 each point (i.e. the center of a crater) and its nearest neighboring point (i.e.
188 the center of the nearest neighbor crater) was determined and averaged, and
189 the mean distance observed was compared with the mean distance expected
190 under random distribution. If the observed value was significantly smaller
191 (greater) than the expected value, the distribution was considered to be
192 significantly clustered (ordered) and not random. This method has been
193 applied to evaluate the distribution of craters on various solar system objects.
194 Phillips et al. (1992) found that, although Venus has a variation in crater
195 density, the variation cannot be distinguished from a completely random
196 distribution; therefore, the variation can be explained by the randomness of
197 the crater production on that planet. Squyres et al. (1997) found that the
198 crater distributions on Callisto and Rhea are not random but are

199 significantly ordered. The spatial distribution of observed craters in heavily
200 cratered terrain transition from random to ordered because craters that form
201 in sparse areas obliterate the relatively few existing craters, filling in the
202 spaces, whereas craters that form in areas of existing crater clustering
203 obliterate the existing craters and reduce the clustering (Lissauer et al.
204 1988; Squyres et al. 1997). Moreover, partial resurfacing such as lava flow or
205 the mass-movement of rock tends to create clustered crater distribution.

206 Following Squyres et al. (1997), the Z value was determined to assess
207 the degree by which the value of the observed mean distance (d_{obs}) deviates
208 from randomness:

$$209 \quad Z \equiv \frac{d_{obs} - d_{exp}}{\sigma}, \quad (1)$$

210 where d_{exp} is the expected mean distance when the distribution is completely
211 random and σ is the standard deviation of d_{exp} . A positive Z value indicates
212 that the distribution of points is ordered, a negative Z value indicates that it
213 is more clustered, and a value of Z close to 0 indicates that the distribution
214 cannot be distinguished from random. A value for Z was obtained for the
215 distribution of all craters that exceeded a given diameter. The Z -statistic was
216 not calculated in cases where the number of craters was lower than $n = 2$.
217 The observed distance between two points was determined on the basis of
218 the great-circle distance between the two points on the unit sphere, although
219 the shape of Ryugu is not spherical. Values for d_{exp} and σ were calculated
220 numerically using the Monte Carlo simulation, following Hirata (2017). This
221 study assumed that (1) n points were produced on the unit sphere, (2) these
222 points were randomly generated because the impactors were assumed to

223 have come from all directions, (3) the mean distance to the nearest neighbor
224 (d_i in i^{th} trial) was measured using the average of the lengths defined by the
225 great-circle distance between two points, (4) based on these three
226 assumptions, 10000 trials were performed, and (5) the average and deviation
227 of d_i ($i = 1, 2, 3, \dots, 10000$) were obtained as d_{exp} and σ , respectively.

228

229 **3. Results**

230 On the surface of Ryugu, 77 craters were identified (Fig. 1); the
231 diameters and locations of these craters are listed in Table 3. Figure 2 shows
232 the global distribution of craters that are bordered with rims as lines on the
233 global mosaic map projected in a simple cylindrical projection. We again
234 confirmed a lack of small craters ($20 \text{ m} < D < 100 \text{ m}$) relative to the number of
235 large craters, as has also been found on other small asteroids such as
236 Itokawa, Eros, and Bennu (Thomas and Robinson, 2005; Michel et al. 2009;
237 Walsh et al. 2019). The largest crater on Ryugu is Urashima, at 290 m in
238 diameter, which is equivalent to 32% of the diameter of Ryugu. The second
239 and third largest craters are Cendrillon (224 m) and Kolobok (221 m),
240 respectively. Only these three craters exceed 200 meters in diameter. The
241 average crater density over Ryugu is 4.4 craters/km² for $D \geq 100 \text{ m}$ and 25.0
242 craters/km² for $D \geq 20 \text{ m}$.

243 The distribution of craters on Ryugu is variable, with differences in
244 crater density depending on longitude and latitude (Fig 3a, b). The Z value
245 (Fig. 3c) suggests that the craters on Ryugu are spatially distributed in
246 clusters, in a statistically significant manner. Therefore, the spatial

247 distribution of craters on Ryugu cannot be explained by the randomness of
248 cratering itself. There are more craters at lower latitudes and fewer craters
249 at higher latitudes (Fig. 3b). Polar regions of greater than 40 degrees latitude
250 have only a few craters. There are more craters around the meridian
251 (300°E-30°E), and fewer at the western bulge (160°E – 290°E). Because of
252 this we termed the region between 300°E-30°E and 40°S-40°N the cratered
253 terrain. The crater density in this region is 57.3 craters/km² ($D \geq 20$ m), twice
254 the global average. However, as shown in Fig 3a, the crater density of the
255 western bulge is roughly half the global average. Although less-cratered
256 terrain is often found both surrounding and on the inside of large craters
257 such as Shoemaker crater on Eros (Robinson et al. 2002), we could not
258 identify any landform that could be associated with a putative large crater at
259 either the polar regions or the western bulge of Ryugu.

260 Ryugu has 11 craters ($D \geq 100$ m), of which 5 cut the crest of the
261 equatorial ridge, Ryujin Dorsum. Note that we concluded that it is unlikely
262 that some of the impact craters found on this ridge did not originate from
263 impacts (i.e., the ridge is a landform made by another mechanism such as
264 mass-movement). This is because the large craters cutting across the ridge
265 (No. 1, 3, 4, 6, 8 in Fig. 1) are all clear and circular bowl-shaped depressions
266 and appear to be distinct impact craters, as discussed by Sugita et al. (2019).
267 We therefore performed a statistical test to evaluate the statistical
268 significance of the concentration of craters on the equatorial ridge, Ryujin
269 Dorsum. Using the Monte Carlo method, we estimated the number of craters
270 expected across the equator under random distribution. In detail: (1) the 11

271 craters exceeding diameters of 100 m, are placed at random points on a
272 sphere with a radius of 448 m using spherical uniform random numbers, (2)
273 the number of craters across the equator is counted, and (3) the average
274 value of the number and its dispersion are obtained from 1000 trials. Results
275 indicate that the expected number of large craters across the equator under
276 random distribution is 2.1 with a dispersion of 1.3. We therefore concluded
277 that the number of observed craters found on the equator (5 craters) was
278 greater than that expected randomly.

279

280 **4. Discussion**

281 Possible explanations for the longitudinal variation in crater density
282 are: (i) resurfacing from processes such as seismic shaking is inert in the
283 cratered terrain and is more active in the western bulge, (ii) differences in
284 the physical terrain inhibit the formation of an impact crater (e.g., Güttler et
285 al. (2012) proposed an armoring effect owing to the presence of boulders),
286 and (iii) the cratered terrain around the meridian (300°E -30°E) is
287 geologically old, while the formation of the western bulge was relatively
288 recent. Seismic shaking or armoring effects, as in (i) and (ii), should
289 theoretically be more effective for smaller craters; however, even large
290 craters on Ryugu show longitudinal variation which indicates that (i) and (ii)
291 are unlikely. We propose that (iii) is the most likely scenario. This is because
292 the western bulge is a geologically distinct terrain, as mentioned in Section 1.
293 The western bulge is proposed to have been caused by the deformation of
294 Ryugu, via a process that occurred on only the western side of the asteroid

295 during a short rotational period of Ryugu in the past, while the eastern
296 hemisphere was left structurally intact (Hirabayashi et al. 2019). On the
297 other hand, Scheeres (2015) proposed that regolith landslides occur on the
298 surface of rapidly spinning asteroids, so the occurrence of such a landslide
299 from the polar regions toward the western hemisphere could be taken into
300 consideration as an alternative explanation for the formation of the western
301 bulge. In addition, such a landslide could be responsible for the latitude
302 variation in crater density (i.e. relatively less-cratered polar regions). In both
303 cases, the crater density of the western bulge represents the timing of the
304 short rotational period of Ryugu, while the cratered terrain around the
305 meridian was already an old surface when the western bulge formed.
306 Probably, the equatorial ridge located in the eastern hemisphere is a fossil
307 structure formed during the short rotational period in the distant past. The
308 ridge that is slightly offset towards the south may indicate a polar shift of
309 Ryugu in the past.

310

311 **5. Conclusion**

312 We have identified 77 craters on the surface of Ryugu. The spatial
313 distribution of the craters on Ryugu is not random, with variations in crater
314 density that can be linked to latitude and longitude; more craters are seen at
315 lower latitudes than at higher latitudes, and there are more craters in the
316 region around the meridian than in the western bulge. The longitudinal
317 variation in crater density could be a possible result of the formation of the
318 western bulge, which is thought to have formed later than the rest of the

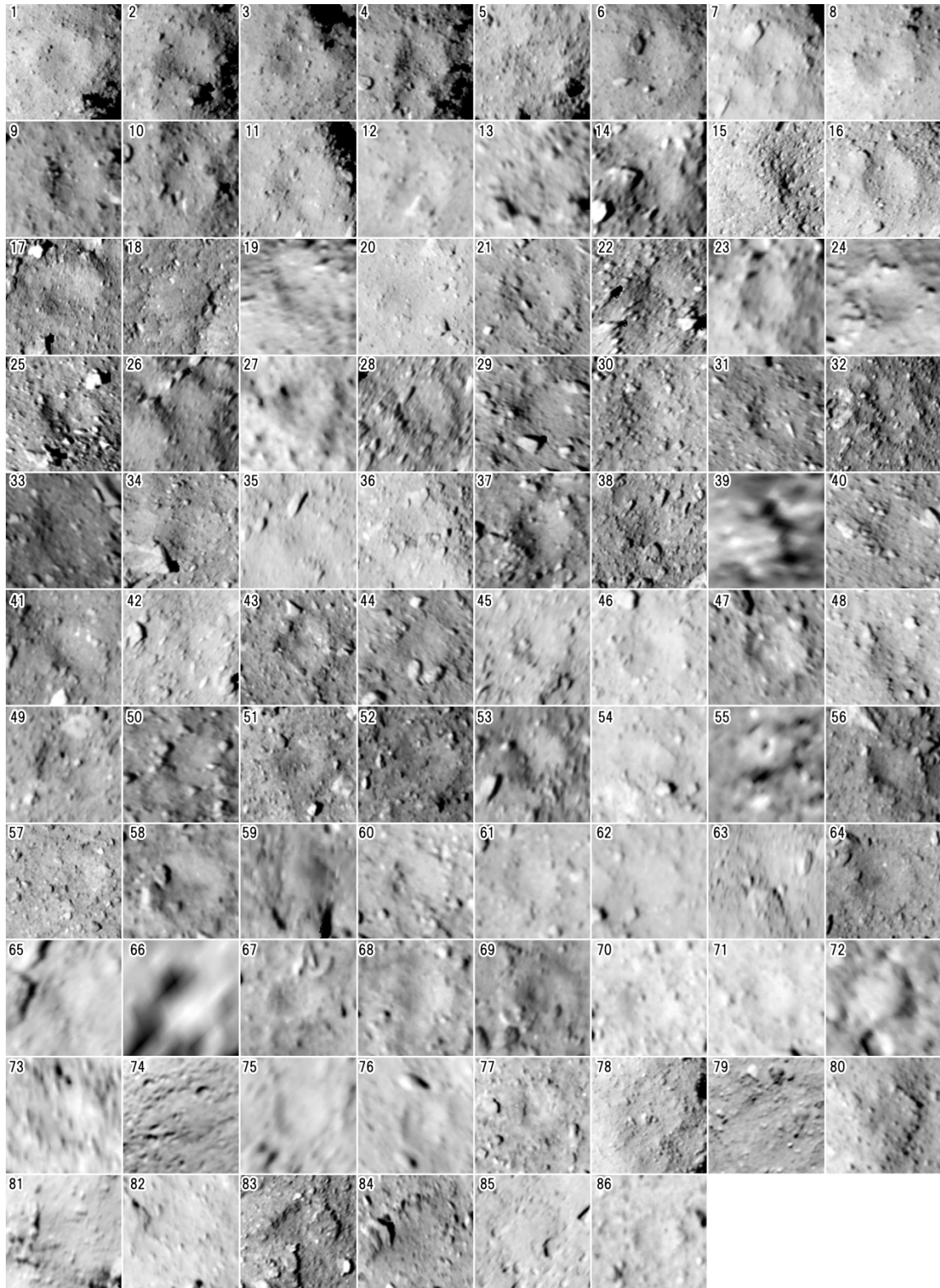
319 asteroid due to its lower proportion of craters. The equatorial ridge located in
320 the eastern hemisphere would be a fossil structure formed during the short
321 rotational period in the distant past.

322

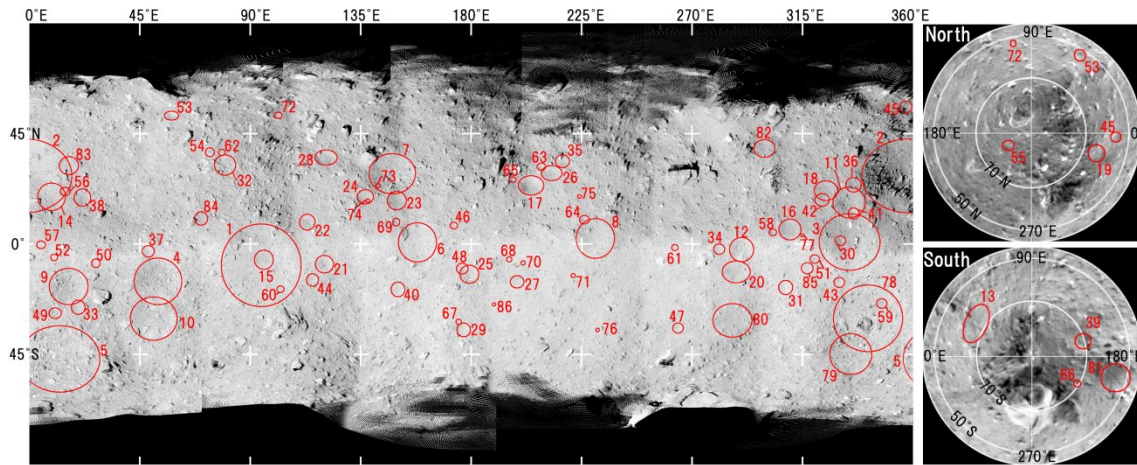
323 **Acknowledgements**

324 This study was supported by the JSPS International Planetary
325 Network. Images obtained by Hayabusa2 will be freely available via Data
326 ARchives and Transmission System (DARTS) at ISAS/JAXA at the end of
327 2020 (<https://www.darts.isas.jaxa.jp/index.html.en>). The shape model of
328 Ryugu has already been released in DARTS. The Small Bodies Mapping Tool
329 has been released at <http://sbmt.jhuapl.edu/index.html>.

330

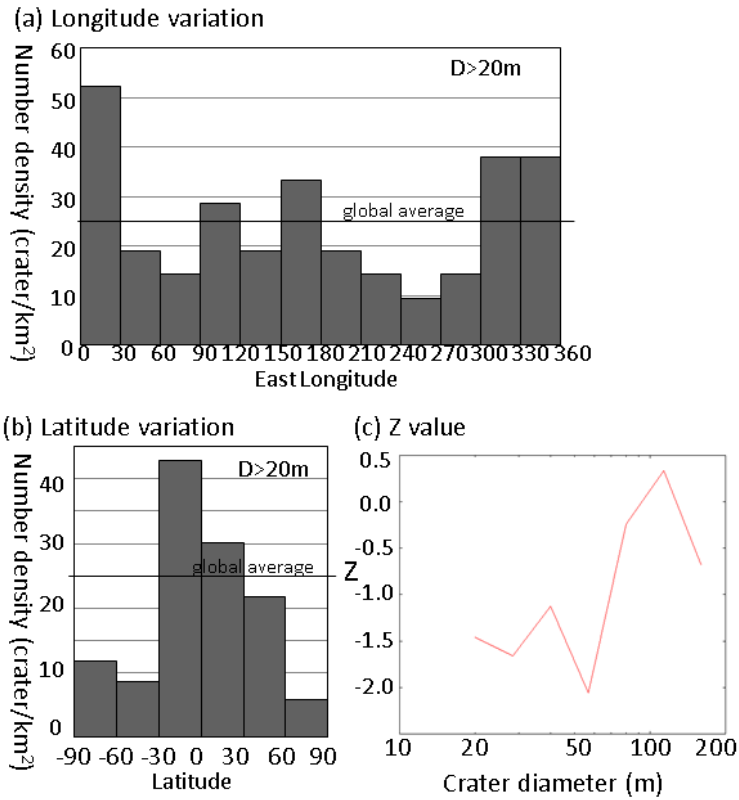


332 **Figure 1.** Candidate craters that were identified. Numbers correspond to
333 those in Table 3.



336 **Figure 2.** The distribution of craters on Ryugu. Red lines roughly outline the
 337 rim of craters. On the left is a simple cylindrical projection mosaic map
 338 derived from the July 20, 2018 images. On the right is the azimuthal
 339 equidistant projection maps centered in the north (top) and south poles
 340 (bottom) derived from January 24, 2019 and August 23, 2018. Numbers
 341 correspond to Figure 1 and Table 3.

342



344 **Figure 3. (a)** The longitudinal variation in crater density ($D \geq 20$ m). **(b)** The
 345 latitudinal variation in crater density ($D \geq 20$ m). **(c)** The Z value for spatial
 346 distribution on Ryugu.

347

348 **Table 1. Images utilized in this work.**

	Date	Num.	Resolution	Note
(i)	Jul. 20 2018	96	0.72 m/px	Low latitude < 70 degree
(ii)	Aug.1 2018	85	0.69-0.55 m/px	Low latitude < 40 degree
(iii)	Oct. 4 2018	11	0.32 m/px	North pole
(iv)	Oct. 30 2018	18	0.62 m/px	North and South poles
(v)	Feb. 28 2019	26	0.67 m/px	North and South poles
(vi)	Aug. 23 2018	52	2.6 m/px	South pole at small emission

(vii)	Jan. 24 2019	52	2.1 m/px	North pole at small emission
-------	--------------	----	----------	------------------------------

349

350 **Table 2.** Classification in this study.

Classification	Characteristic	Our Judge
I	Circular depression with rim	Crater
II	Circular depression without rim	Crater
III	Quasi-circular depression	Crater
IV	Quasi-circular features	Not crater

351

352 **Table 3.** Impact craters on Ryugu

# ^{*1}	Lat.	Lon. (°E)	D (m)	CL ^{*2}
<i>Classification I-III</i>				
1	-7.19	92.99	290	I
2	28.34	353.68	224	II
3	-0.70	330.28	221	II
4	-14.83	51.20	183	I
5	-50.56	9.84	173	III
6	0.42	157.84	154	II
7	30.37	145.99	145	II
8	3.24	229.95	142	I
9	-17.19	14.29	133	II
10	-31.50	47.26	131	I
11	17.02	332.23	100	I
12	-1.88	289.49	90.2	II
13	-63.73	24.45	85.0	III
14	16.90	6.44	79.0	III
15	-4.54	95.52	78.9	III
16	6.01	308.75	77.1	I
17	23.70	205.33	76.2	II
18	20.86	322.68	73.9	II
19	57.73	342.98	73.3	II

20	-11.64	287.71	69.0	III
21	-8.44	119.53	69.0	I
22	8.28	111.52	65.8	III
23	18.59	149.73	65.8	II
24	19.65	136.94	62.1	II
25	-12.18	179.11	61.0	II
26	28.48	213.16	58.2	II
27	-16.28	199.13	53.6	II
28	36.81	121.83	52.2	III
29	-36.18	176.65	51.3	III
30	-0.07	329.24	51.3	II
31	-17.20	307.19	48.8	II
32	33.09	81.45	48.4	III
33	-26.28	17.83	46.6	II
34	-1.87	279.89	44.2	II
35	33.50	217.25	44.1	III
36	24.37	335.50	43.1	III
37	-3.08	47.02	42.7	I
38	18.62	20.92	42.5	III
39	-69.03	170.39	41.7	III
40	-19.49	150.94	41.4	III
41	11.91	334.53	39.9	I
42	17.52	323.27	39.7	II
43	-15.38	328.28	37.2	II
44	-14.87	115.35	36.5	II
45	55.75	357.50	36.0	II
46	7.79	173.00	34.6	I
47	-34.51	263.82	34.4	I
48	-10.68	176.31	32.0	II
49	-28.57	9.83	30.6	III
50	-7.92	26.75	29.3	III
51	-6.30	319.67	28.1	III
52	-5.81	9.76	27.6	III
53	52.36	57.31	27.5	II
54	37.10	73.44	26.5	III
55	79.00	209.00	26.0	II

56	21.44	13.71	25.3	III
57	-0.89	4.52	24.4	III
58	4.61	301.74	23.6	I
59	-24.00	346.55	21.7	III
60	-19.26	102.14	21.5	III
61	-2.08	263.10	21.0	II
62	37.02	78.22	20.9	III
63	31.21	208.26	20.2	III
64	8.40	225.72	17.2	I
65	25.81	196.97	16.2	II
66	-69.00	211.00	16.0	II
67	-31.59	174.66	14.5	II
68	-6.96	195.40	14.4	III
69	9.65	149.10	14.0	I
70	-8.37	201.10	14.0	II
71	-12.89	221.27	13.9	II
72	52.43	100.93	12.6	II
73	23.18	141.89	12.5	II
74	17.15	137.76	11.4	II
75	19.01	224.05	11.2	II
76	-35.88	231.29	10.5	II
77	3.40	314.61	10.0	II
<i>Classification IV</i>				
78	-31.21	341.74	223	IV
79	-45.92	334.99	133	IV
80	-30.64	284.23	112	IV
81	-58.37	198.43	112	IV
82	38.21	298.88	55.8	IV
83	31.87	15.43	53.0	IV
84	10.26	69.87	46.7	IV
85	-10.59	316.99	35.0	IV
86	-25.36	189.21	11.4	IV

353 *1 Number in descending order of diameter. Ryugu has 7 named craters:
354 Urashima (No.1), Cendrillon (No.2), Kolobok (No.3), Momotaro (No.4),
355 Kintaro (No. 6), Brabo (No. 8), and Kibidango (No.10).

356 *2 Classification shown in Table 2.

357

358 **References**

359 Güttler, C., N. Hirata, and A.M. Nakamura (2012) Cratering experiments on
360 the self armoring of coarse-grained granular targets. *Icarus* 220(2),
361 1040-1049.

362 Hirabayashi et al. (2019), The Western Bulge of 162173 Ryugu Formed as a
363 Result of a Rotationally Driven Deformation Process. *The*
364 *Astrophysical Journal Letters* 874, Number 1.

365 Hirata N. (2017) Spatial distribution of impact craters on Deimos. *Icarus* 288,
366 69-77.

367 Kahn, E. G., O. S. Barnouin, D. L. Buczkowski, C. M. Ernst, N. Izenberg, S.
368 Murchie and L. M. Prockter. (2011) A Tool for the Visualization of
369 Small Body Data. In *42nd Lunar and Planetary Science Conference*,
370 Abstract #1618. Houston: Lunar and Planetary Institute.

371 Lissauer, J. J., S. W. Squyres, and W. K. Hartmann (1988), Bombardment
372 History of the Saturn System, *Journal of Geophysical Research: Solid*
373 *Earth*, 93(B11), 13776-13804.

374 Michel, P., D. P. O'Brien, S. Abe, and N. Hirata, (2009) Itokawa's cratering
375 record as observed by Hayabusa: implications for its age and
376 collisional history. *Icarus* 200, 503–513.

377 Phillips, R. J., R. F. Raubertas, R. E. Arvidson, I. C. Sarkar, R. R. Herrick, N.
378 Izenberg and R. E. Grimm (1992) Impact craters and Venus
379 resurfacing history. *Journal of Geophysical Research: Planets* 97,

380 15923-15948.

381 Robinson, M. S., P. C. Thomas, J. Veverka, S. L. Murchie, and B. B. Wilcox
382 (2002) The geology of 433 Eros. *Meteoritics & Planetary Science*
383 37(12), 1651-1684.

384 Scheeres, D.J., (2015) Landslides and Mass shedding on spinning spheroidal
385 asteroids. *Icarus* 247, 1-17.

386 Squyres, S. W., C. Howell, M. C. Liu and J. J. Lissauer (1997) Investigation
387 of Crater “Saturation” Using Spatial Statistics. *Icarus* 125, 67-82.

388 Sugita, S. et al. (2019) The geomorphology, color, and thermal properties of
389 Ryugu: Implications for parent-body processes. *Science* 364, 272-275.

390 Thomas, P. C. and M.S. Robinson, (2005) Seismic resurfacing by a single
391 impact on the asteroid 433 Eros. *Nature* 436, 366–369.

392 Walsh, K. J. et al. (2019), Craters, boulders and regolith of (101955) Bennu
393 indicative of an old and dynamic surface. *Nature Geoscience* 12, 242–
394 246.

395 Watanabe S. et al. (2019) Hayabusa2 arrives at the carbonaceous asteroid
396 162173 Ryugu—A spinning top-shaped rubble pile. *Science* 364,
397 268-272.